Variability and Energetics of the Kuroshio Extension and Its Recirculation Gyre from the First Two-Year TOPEX Data*

BO QIU

Department of Oceanography, University of Hawaii at Manoa, Honolulu, Hawaii

(Manuscript received 17 October 1994, in final form 5 December 1994)

ABSTRACT

Altimetry data from the first 21-month TOPEX mission (September 1992–June 1994) are analyzed to investigate the sea surface height (SSH) fluctuations in the Kuroshio Extension and its southern recirculation gyre regions (25°–40°N, 136°E–180°). To separate the time-dependent (SSH) signals associated with the Kuroshio Extension from those associated with the westward recirculating flows, and to study the energetics of these currents, the author first estimated the mean SSH profiles along individual ground tracks by assuming the velocity profile of the Kuroshio Extension to be Gaussian shaped and by successively fitting the synthetic current's height profile to the time-dependent SSH data. The mean SSH field, including the influence from the recirculating flows, is then derived through the constraint from climatological hydrographic data.

During the 21-month period of the TOPEX mission, the eddy kinetic energy (EKE) of the Kuroshio Extension had relatively uniform values during three separate stages, each of which lasted longer than 6 months. A significant drop in the EKE level is found in the Kuroshio Extension after the end of 1993. In contrast, the EKE level in the southern recirculation region increased steadily over the two-year period. The energetics analysis shows that this EKE increase is due to the energy transfers from the mean flow field to the eddy field through barotropic instabilities. These barotropic eddy processes are found to be less important for the EKE changes in the Kuroshio Extension and its northern areas. On both seasonal and interannual timescales, the large-scale path fluctuations of the Kuroshio Extension are found to correlate significantly with the surface transport fluctuations: a more northerly Kuroshio Extension tends to correspond to a larger surface transport. Over the two-year period, both the eastward-flowing Kuroshio Extension and the westward recirculating flows weakened steadily. This decline in the intensity of the recirculation gyre is caused by the energy transfers from the mean flow field to the eddy field occurring in the region south of the Kuroshio Extension.

1. Introduction

Satellite radar altimetry is a powerful observational tool for monitoring mesoscale to large-scale sea surface height (SSH) fluctuations. Its potential use in improving ocean predictability through data assimilation in numerical models is also a subject of increasing interest. Due to the small ratio of the geographical changes in the mean SSH (1–2 m at most) to those of the earth's gravitational field (~100 m, typically), the mean SSH signal is usually lost when the unknown geoid is removed. For many oceanographic applications, however, the absolute (mean plus the time varying) SSH information is desirable and this is particularly true for studies focusing on western boundary current regions, where the mean SSH is comparable to the time-varying SSH. For these regions, mean SSH derived from climatological hydrographic data, such as those by Levitus (1982), cannot substitute for the mean SSH that is pertinent to a satellite altimetric mission. This is both because of the significant interannual changes in the boundary currents and because of the uncertainty in specifying the reference velocities.

To obtain the mean SSH field of the Kuroshio Extension pertinent to the 2.5-year period of the Geosat Exact Repeat Mission (ERM), Qiu et al. (1991) applied the kinematic jet model of Kelly and Gille (1990), which reconstructs the along-track mean SSH profile from the residual SSH data, to all ground tracks in the region of 30°–40°N, 140°E–180°. They determined the two-dimensional mean SSH field in this region by combining the mean height profiles along the ascending and descending tracks through an inversion. The mean SSH field thus estimated recovers the mean Kuroshio Extension with a sharp cross-stream resolution, and its general pattern is found to agree favorably with those presented by Mizuno and White (1983) and Teague et al. (1990) based on historical XBT and hydrographic data. Using the mean SSH data and the residual SSH data from the 2.5-year Geosat ERM, Qiu et al. discussed in detail the mean-versus-eddy kinetic energy distributions, the eddy propagations, and the seasonal/

* SOEST Contribution Number 3881.

Corresponding author address: Dr. Bo Qiu, Department of Oceanography, University of Hawaii at Manoa, 1000 Pope Rd., Honolulu, HI 96822.

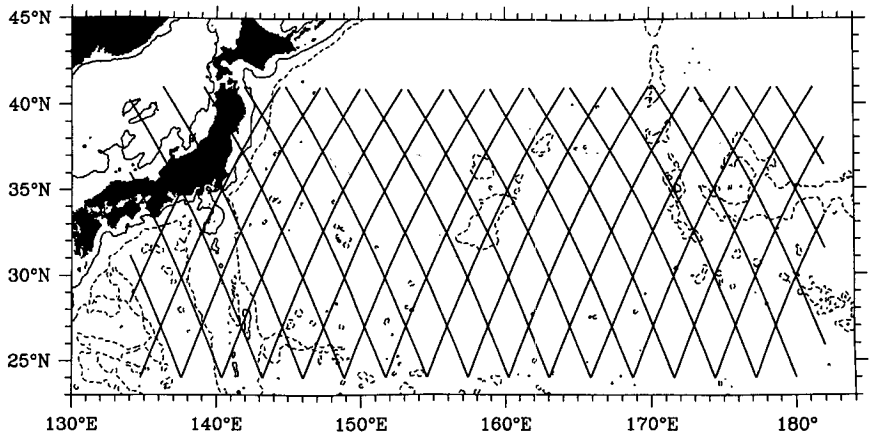

FIG. 1. Distribution of the TOPEX ascending and descending tracks used in this study. Dashed lines denote the 4000-m isobaths, and thin solid lines the 1000-m isobaths. Major bathymetric features in this region include the Izu–Ogasawara Ridge along 140°E, the Shatsky Rise near 159°E, and the Emperor Seamounts along 172°E.

interannual changes associated with the Kuroshio Extension. Using different approaches, Tai (1990), Zlotnicki (1991), and Mitchell et al. (1994) have also looked into the eddy propagation and the seasonal signal of the Kuroshio Extension for the Geosat ERM period. Common features obtained from the above studies include that the mesoscale eddies in the Kuroshio Extension region propagate generally westward with speeds of long baroclinic Rossby waves and that the surface transport of the Kuroshio Extension has a maximum in late summer and a minimum in spring.

In this study, we will use the altimeter data obtained from the ongoing TOPEX mission; we will focus not only upon the Kuroshio Extension itself, but also on its southern recirculation gyre. Like the Gulf Stream system in the North Atlantic, when compared with its upstream value in the East China Sea, the transport of the Kuroshio and Kuroshio Extension doubles in the downstream deep basin of the Pacific Ocean. Such a downstream increase in transport is attributable to the presence of westward recirculating flows (e.g., Masuzawa 1972; Kawai 1972). A better understanding of the variability of the Kuroshio Extension clearly requires examination of these recirculating flows. Despite its importance for the upper-ocean heat balance in the Kuroshio Extension region (Qiu and Kelly 1993) and for the mode water distributions south of Japan (Suga et al. 1989), variability of the recirculating flows in the Kuroshio and Kuroshio Extension system is not well understood. In the past, lack of an onboard radiometer and the existence of relatively large measurement errors have prevented us from using the Geosat data to examine the interaction of the Kuroshio Extension and its recirculating flows (the latter have typical SSH signals of about 10 cm). With the improved measurement precision of the TOPEX altimeter (that is, an rms SSH error of 3 cm), it is now possible to address this question. As we will find below, clarifying the changes in the recirculating flows is crucial to our understanding of the low-frequency changes in the Kuroshio Extension.

Following a brief description on the TOPEX data processing in the next section, we will describe in section 3 a method that extends the kinematic jet model to include the effect of the westward recirculating flows for determining the along-track mean SSH profiles. The result of the two-dimensional mean SSH field pertinent to the first two-year period of the TOPEX mission is then presented. In section 4, we will describe the changes in the eddy kinetic energy field and examine the energy transfers between the mean flow field and the eddy field. Section 5 focuses on the large-scale, low-frequency fluctuations of the Kuroshio Extension; in particular, we will look into the surface transport changes of the Kuroshio Extension and their connections with the path changes of the Kuroshio Extension and the changes in the southern recirculation gyre. Results from the present study will be summarized in section 6.

2. Altimeter data processing

The first 64 cycles of the TOPEX altimeter data, from October 1992 through June 1994, are used in this study. No data from the Poseidon altimeter are included here because significantly fewer passes were obtained from the Poseidon altimeter during this time period. To focus on the Kuroshio Extension and its southern recirculation gyre, all ascending and descending ground tracks from 25° to 40°N and from 136°E to 180° are processed (see Fig. 1).

For each of the 36 selected ground tracks, we first adjust the raw TOPEX height data for various environmental corrections, including the tides and the in-

verse barometer effect, according to the GDR users handbook (Callahan 1993). In addition to these recommended corrections, a 60-day harmonic is further removed from the along-track height data. By comparing the TOPEX altimeter and numerous WOCE sea level station time series, Mitchum (1994) showed that the removal of the 60-day harmonic can minimize aliased M_2 and S_2 tidal energy and significantly improve the linear correlation between the two time series. After these corrections, the height data are interpolated to a common latitude grid with a one-per-second sample rate (about 5.6 km along a ground track). The along-track residual SSH profiles $h'(y, t)$ are then calculated by subtracting from each height profile the temporally averaged profile (namely the geoid plus the two-year mean SSH). Finally, a low-pass filter, which has a half-power point at 52 km, is applied to the residual SSH profiles to suppress small-scale instrumental noises. This low-pass filtering has little influence upon the mesoscale, oceanic signals that are of interest to this study. Figure 2a shows some examples of the low-pass filtered residual height profiles along the TOPEX track p075. This track overpasses the point 34°N, 145.5°E (cf. Fig. 1).

3. Reconstructing the mean SSH field

We start with a short review of the kinematic jet model proposed by Kelly and Gille (1990). The basic idea of the kinematic jet model is as follows: due to the large lateral excursions of a boundary current, the mean SSH profile across the current has a more gradual slope than the instantaneous height profiles. Assuming the boundary current has a Gaussian-shaped instantaneous surface velocity profile

$$u_s(y, t) = a_1(t) \exp\left[\frac{-(y - a_2(t))^2}{2a_3(t)^2}\right], \qquad (1)$$

this distinctive slope characteristic enables us to estimate the boundary current's position a_2, width a_3, and strength a_1 from the altimetrically derived residual height data $h'(y, t)$, where y denotes the along-track

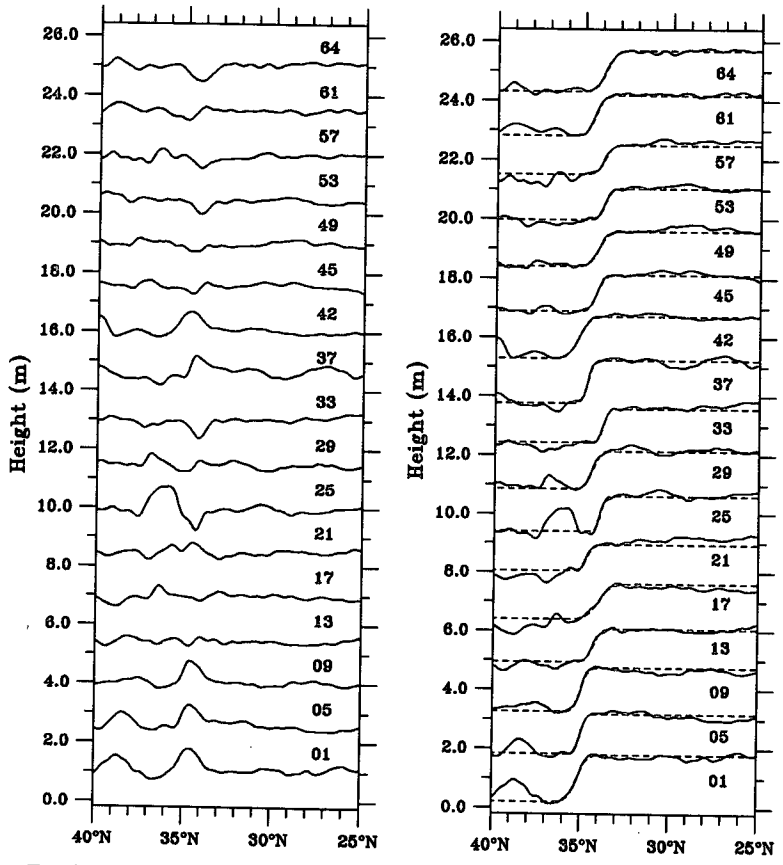

FIG. 2. (a) Typical residual SSH profiles $h'(y, t)$ measured by the TOPEX altimeter. These profiles are along the ascending track p075, which overpasses the point (34°N, 144.5°E). Each height profile is plotted with an offset of 1 m, and the cycle number of TOPEX is denoted to the right. (b) Synthetic height profiles (dashed lines) and the profiles of the residual SSH plus the synthetic mean height (solid lines) after the kinematic jet model is applied to the residual height data from 64 cycles along the track p075.

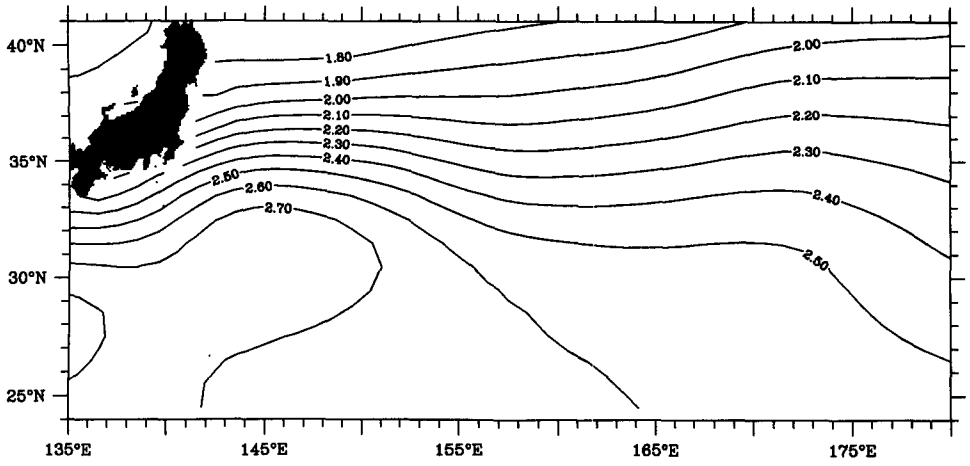

FIG. 3. Climatological mean of the sea surface dynamic height field relative to a 2000-m depth (Levitus 1982). The height values along 25° and 40°N are used in this study to constrain the total surface transport of the Kuroshio Extension system. Units are meters.

distance. For example, the initial guess for the Kuroshio Extension's axis in Fig. 2a can be made where $-\partial h'(y, t)/\partial y$ is locally maximum.

From geostrophy, the synthetic height profile of the boundary current in Eq. (1) is

$$h_s(y, t) = -\frac{f}{g} a_1(t) a_3(t) \sqrt{\pi/2}\, \mathrm{erf}\left[\frac{y - a_2(t)}{\sqrt{2} a_3(t)}\right], \quad (2)$$

where $\mathrm{erf}(y)$ is the error function, and the temporal average of these synthetic height profiles gives an estimate of the mean SSH profile $\overline{h_s}(y)$. Iteratively minimizing the difference between the individual synthetic height profile $h_s(y, t)$ and the profile of the residual SSH plus the synthetic mean improves the estimates for $a_i(t)$ and, consequently, the profile of $\overline{h_s}(y)$. It can be shown that $\overline{h_s}(y)$ converges to the mean SSH profile if the boundary current's position changes are comparable to the current's mean width (Qiu 1992). Figure 2b gives examples of the synthetic height profiles (dashed lines) and the profiles of the residual SSH plus the synthetic mean (solid lines) after this method is applied to the TOPEX data shown in Fig. 2a.

Notice that the kinematic jet model assumes that the height jump associated with the eastward boundary current remains unchanged away from the jet. This results in a level mean SSH outside the meandering range of the boundary current. In the actual mean flow field adjacent to the Kuroshio Extension, recirculation gyres and ambient large-scale flows have been observed (Masuzawa 1972; Joyce and Schmitz 1988), which can cause the mean SSH field to undulate away from the Kuroshio Extension. One way of recovering these relatively weak mean flows is to modify the synthetic mean SSH profile $\overline{h_s}(y)$ through constraint of available hydrographic data. For the current system of the Kuroshio Extension, we assume that the mean SSH profile along each TOPEX track from 25° to 40°N is given by the sum of the synthetic mean SSH, a constant offset c, and possible modifications by the large-scale mean circulations on the two sides of the Kuroshio Extension:

$$h_m(y) = \overline{h_s}(y) + c - [\alpha \mathrm{H}(y - y_m) + \beta \mathrm{H}(y_m - y)] \times (y - y_m)\left[1 - \exp\frac{-(y - y_m)^2}{2(4\sigma)^2}\right], \quad (3)$$

where $y_m = \overline{a_2(t)}$ is the mean axis position of the Kuroshio Extension, σ is the standard deviation of $a_2(t)$, and $\mathrm{H}(y)$ is the Heaviside step function. In Eq. (3), α and β are the slope parameters associated with the large-scale mean circulations on the northern side and southern side of the Kuroshio Extension, respectively. The factor $1 - \exp[-(y - y_m)^2/2(4\sigma)^2]$ in Eq. (3) forces the last term to vanish near the mean path of the Kuroshio Extension, where the mean SSH is adequately captured by the kinematic jet model. The constant offset c is defined as the h_m value at $y = y_m$.

To determine the slope parameters α and β, we require that $h_m(y)$ at the two end points, $y = 25°$ and 40°N, match the sea surface dynamic height values in the Levitus (1982) climatology (see Fig. 3). The rationale for this is that away from the energetic Kuroshio Extension, the mean SSH field has relatively large spatial scales and the Levitus climatology, though highly smoothed, can provide reasonable estimates for the mean SSH values. Notice that this requirement only constrains the total surface transport from 25° to 40°N. The detailed along-track pattern of the mean SSH, and the transports associated with the eastward-flowing Kuroshio Extension and the recirculation gyre, are determined by the TOPEX data.

In this study, the above kinematic jet model is applied to the 36 TOPEX tracks shown in Fig. 1. Due to

the stable path of the Kuroshio west of 136°E (see Taft 1972; Kawabe 1985), no reliable $\overline{h_s}(y)$ are obtained for the westernmost one ascending and two descending tracks. The two-dimensional SSH mean field is, thus, estimated from the remaining 33 ascending and descending tracks. It is worth mentioning that the along-track mean SSH value is a relative quantity: choosing any constant offset c in Eq. (3) will not alter the pattern of the cross-track velocity. This constant becomes important, however, if we are to determine the two-dimensional field of the mean SSH. In this study, c (=2.38 m) is chosen such that the rms difference between the h_m values from the ascending and descending tracks averaged over all crossover points in the model domain is minimum.

Figure 4 shows the objectively mapped mean SSH field from the $h_m(y)$ profiles that are individually estimated using the TOPEX and Levitus data. The zonal and meridional decorrelation scales for the mapping are 3° longitude and 1° latitude, respectively. The SSH gradient of the mean Kuroshio Extension in Fig. 4 is much sharper (by a factor of 2) than its counterpart in Fig. 3. One obvious reason for this is that the Kuroshio Extension is well sampled in the cross-stream direction by the TOPEX altimeter, which allows the use of a smaller meridional decorrelation scale in mapping the mean SSH field. To the south of the Kuroshio Extension, Fig. 4 reveals the existence of a well-defined anticyclonic recirculation gyre. This gyre is only vaguely discernible in the Levitus data. Since the recirculating flows have a significant barotropic component (Schmitz et al. 1987; Joyce and Schmitz 1988), this discrepancy is attributable to the fact that Fig. 4 gives the absolute mean SSH, whereas the mean SSH in Fig. 3 is referenced to the 2000-m depth.

The general picture of the mean SSH field derived from the two-year TOPEX data, including the two quasi-stationary meanders east of Japan and broadening of the path after the Kuroshio Extension encounters the Shatsky Rise around 159°E, agrees well with the picture derived from the Geosat ERM data (Qiu et al. 1991, their Fig. 3a). Because detailed descriptions of the mean Kuroshio Extension and comparisons with existing observations were given in that study, they will not be pursued further here. Figure 5 shows examples of the absolute (mean plus the residual) SSH field in the two year period of the TOPEX mission. Here, the residual height field is derived by objectively mapping the available TOPEX data in both time and space. The zonal and meridional decorrelation scales for the mapping are 3° and 1°, respectively, and the temporal decorrelation scale is 20 days.

4. Eddy kinetic energy and energetics

Using the along-track gradient of the residual SSH data, we calculate the eddy kinetic energy (EKE) of the surface flow. Because the time-dependent velocity field is nearly isotropic in the surface Kuroshio Extension (Schmitz et al. 1987; Hall 1989), the EKE is defined here by the average of the squared cross-track velocity components from ascending and descending tracks. Figure 6a shows the time series of the EKE averaged in the model domain (25°–40°N, 136°E–180°). It is clear from Fig. 6a that the EKE level, when averaged over the model basin, changed from a period of low value ($\sim$0.065 m^2 s^{-2}) to a period of relatively high value ($\sim$0.080 m^2 s^{-2}) and then dropped back to the level of $\sim$0.065 m^2 s^{-2}. Each of these periods, in which the energy level is more or less constant (denoted hereinafter as period I, II, and III), lasted for 6 months or longer. Given these observed changes in the EKE level, two questions immediately arise: First, are these changes associated with the Kuroshio Extension fluctuations or with the fluctuations in the ambient flow field? Second, what are the possible mechanisms that cause these low-frequency shifts in the EKE level?

We start with the first question. As depicted in Fig. 2, one output from the kinematic jet model is the axis

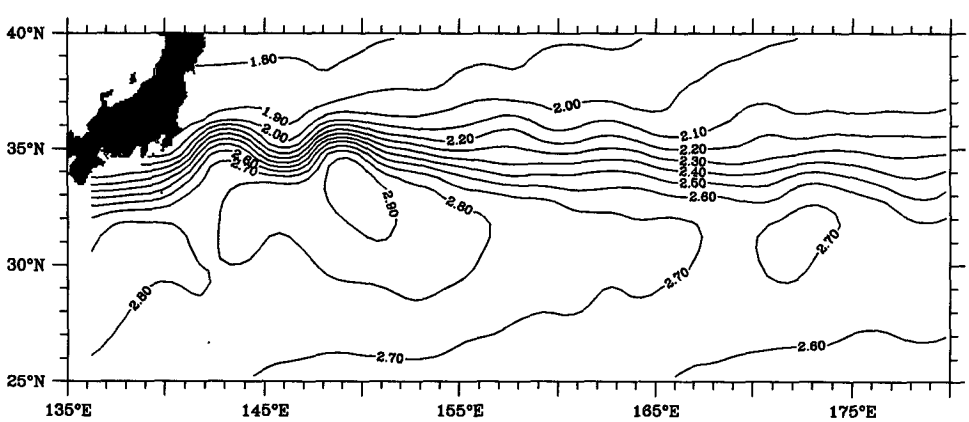

FIG. 4. Mean SSH field estimated from the first 64 cycles of the TOPEX data (October 1992–June 1994). The height field is objectively mapped from the mean height profiles that are independently estimated along the ascending and descending tracks (Fig. 1).

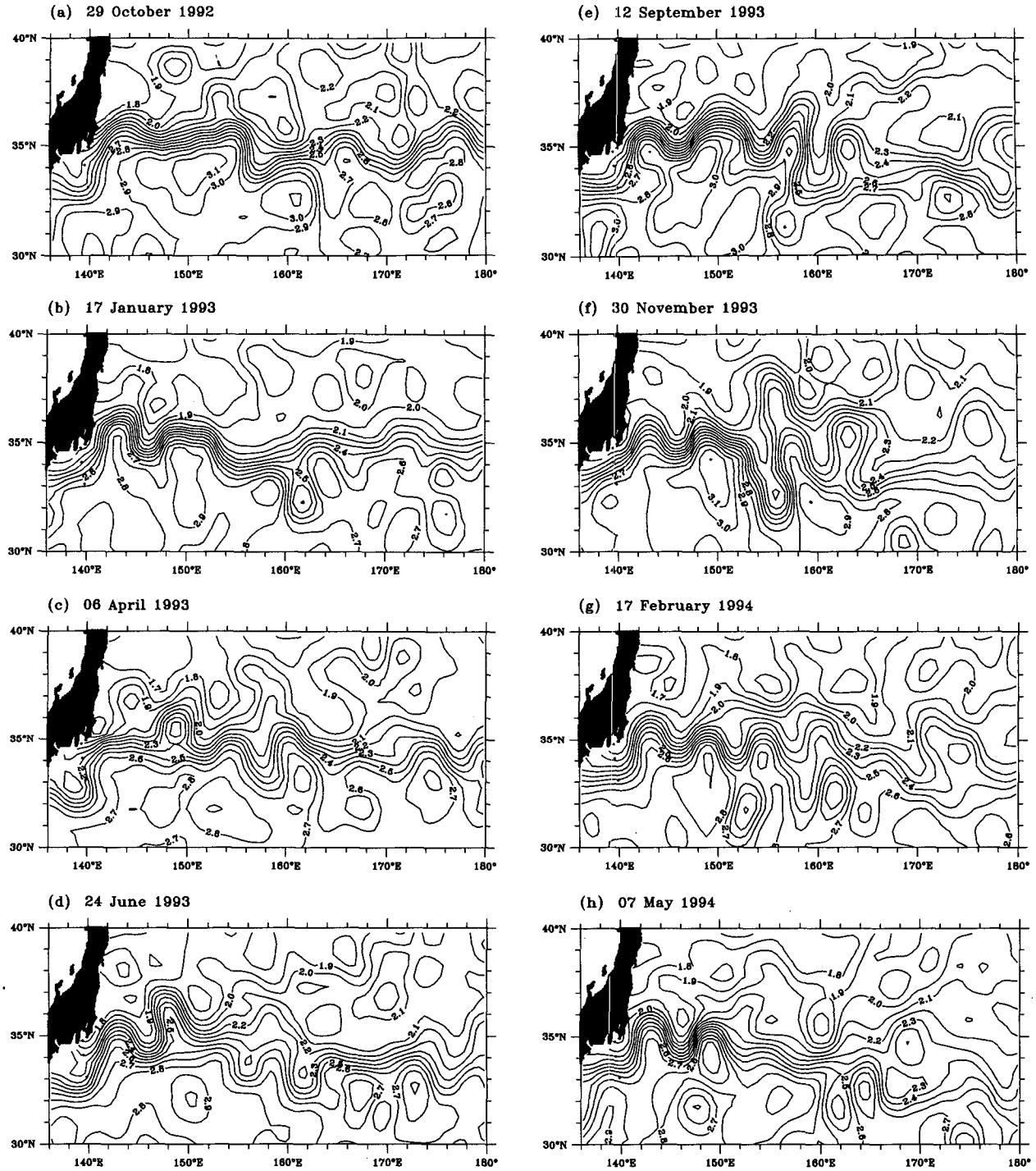

FIG. 5. Sea surface height fields obtained by adding the objectively mapped residual SSH data to the mean SSH field shown in Fig. 4. Units are meters.

position of the Kuroshio Extension for the individual tracks and cycles. If we assume that the Kuroshio Extension has a typical width of 3° in latitude, it is possible to separate the residual SSH data into the region of the Kuroshio Extension, the region south of the Kuroshio Extension, and the region to the north. For each of these regions, we compute the time series of the averaged EKE (Figs. 6b–d). Interestingly, the well-defined, 3-step change of the EKE found in Fig. 6a is less obvious when placed among these separated time series.

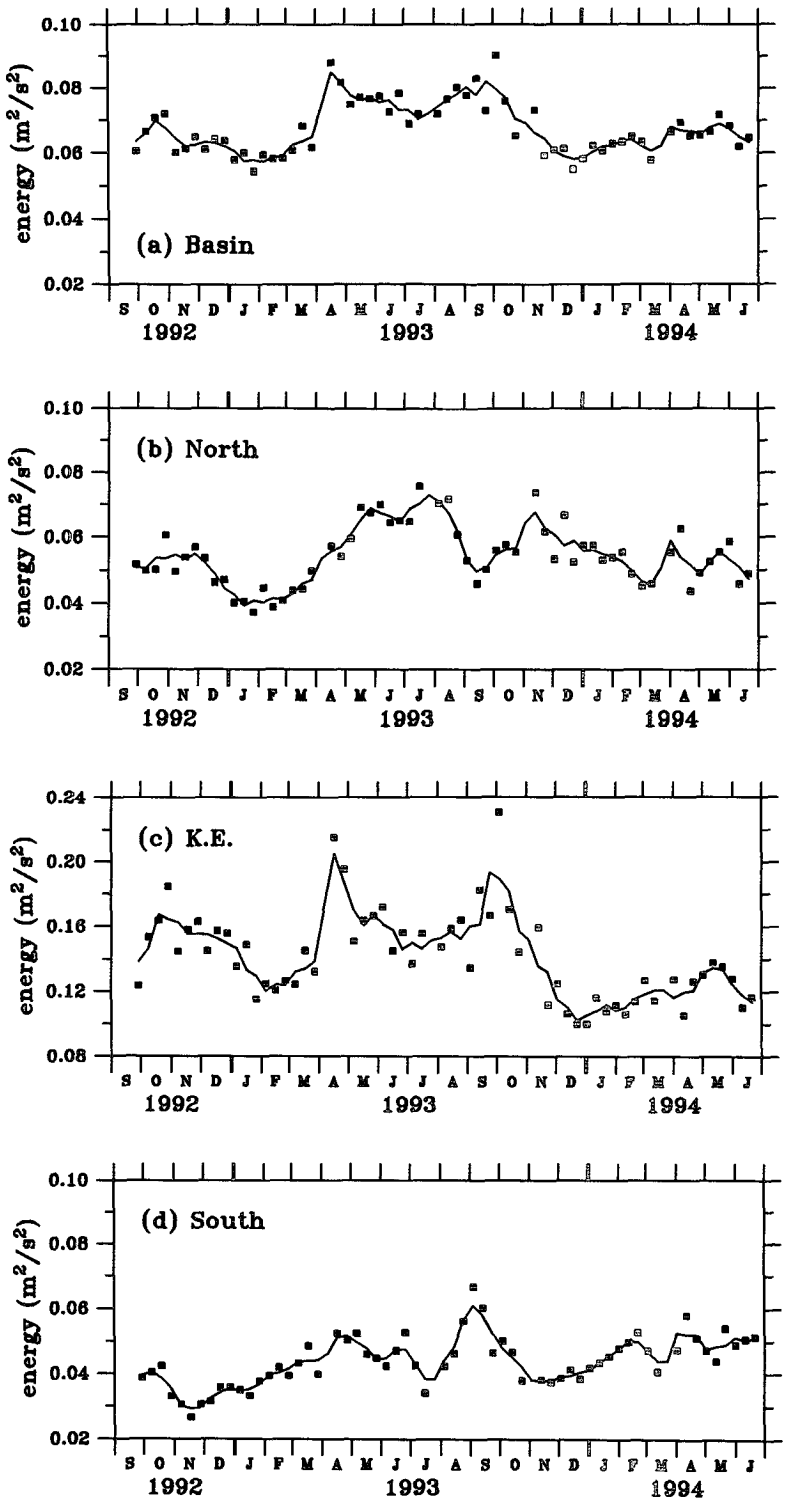

FIG. 6. Time series of the eddy kinetic energy (EKE) averaged in (a) the entire area of the model basin (25°–40°N, 136°E–180°), (b) the region north of the Kuroshio Extension, (c) the Kuroshio Extension, and (d) the region south of the Kuroshio Extension. Solid marks denote the EKE values averaged for all tracks in each TOPEX cycle. Because the neighboring tracks in the same cycle can be separated by as long as 10 days, the EKE values averaged over the consecutive 3 cycles are shown in the figures by solid lines.

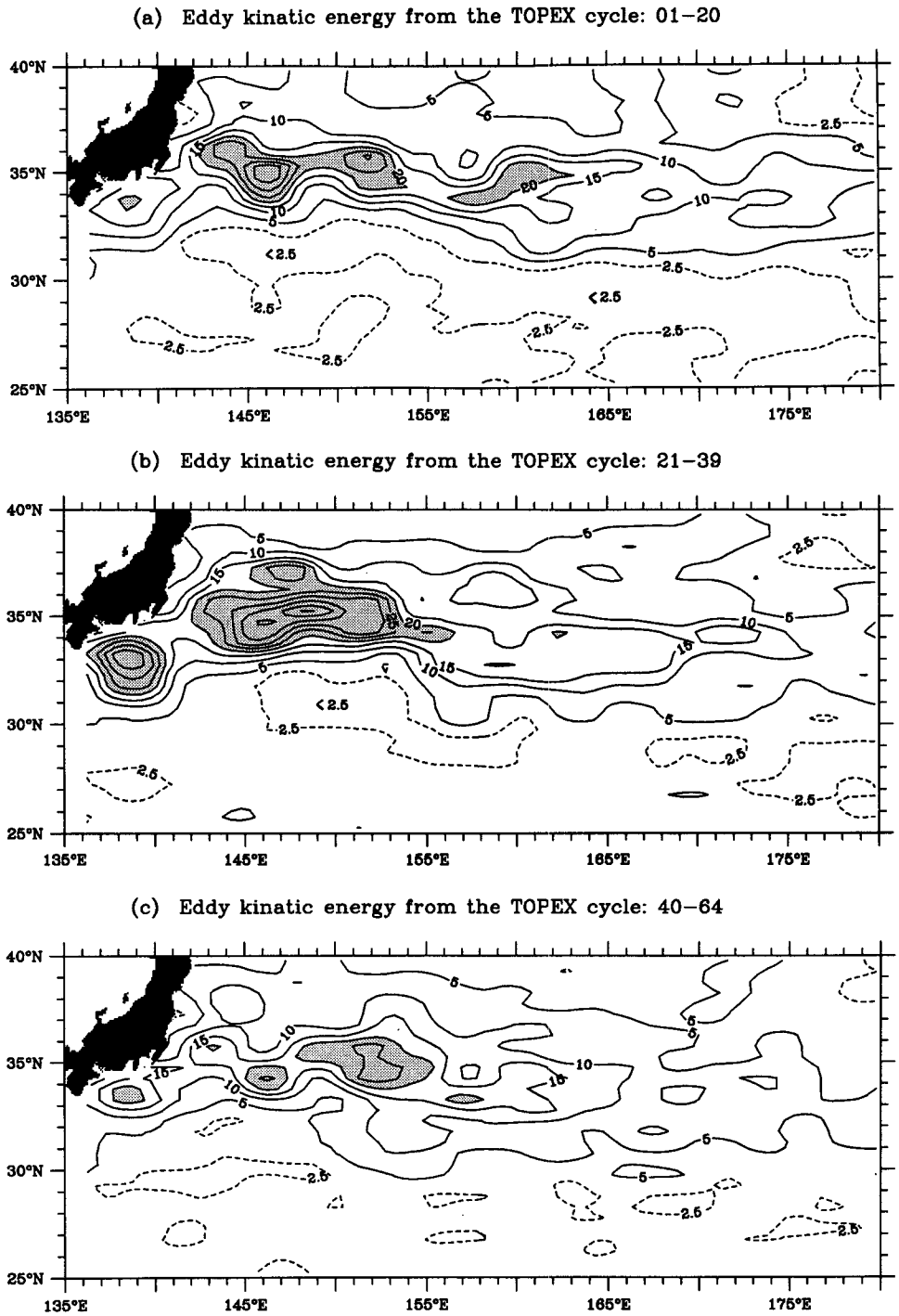

FIG. 7. Eddy kinetic energy distribution calculated from the residual SSH data for the TOPEX cycle: (a) 01–20, (b) 21–39, and (c) 40–64. The contour unit is 0.01 $m^2 s^{-2}$, and areas with energy level greater than 0.2 $m^2 s^{-2}$ are stippled.

The EKE in the Kuroshio Extension, which is dominant in the three regions, exhibits a remnant of the 3-step changes, but the energy level within each step is less uniform. In fact, the difference in the averaged energy level between period I and II appears smaller, and the energy level in these two periods is considerably higher than it is in period III. In contrast to Fig. 6c, the EKE associated with the southern recirculation gyre in Fig. 6d shows a trend opposite to that of the Kuroshio Extension: the EKE level increased more or less steadily

over the two-year period of the TOPEX mission. A least-squares fit reveals the linear trend to be $(0.256 \pm 0.052) \times 10^{-9}$ m^2 s^{-3}, or about 0.008 m^2 s^{-2} per year, for the EKE increase. The EKE time series in the region north of the Kuroshio Extension (Fig. 6b) has a pattern similar to that in Fig. 6d: the EKE level is low in period I as compared to the subsequent periods. However, no statistically significant linear trend is found in the time series for this northern region [the least squares fit gives $(0.077 \pm 0.072) \times 10^{-9}$ m^2 s^{-3} for the slope].

These energy-level changes can also be easily detected if we plot the EKE distributions averaged in these three time periods respectively (Figs. 7a–c). In the Kuroshio south of Japan and in the upstream Kuroshio Extension, for example, there is a clear EKE-level increase from period I to period II. Farther downstream near the Shatsky Rise, around 160°E, the energy level decreased somewhat from period I to II. In period III, Fig. 7c shows a definite decrease in the EKE level throughout the path of the Kuroshio Extension. This was reflected clearly in the time series of Fig. 6c. The fact that the EKE maxima of the Kuroshio occur in regions south of Japan, in the upstream Kuroshio Extension where the quasi-stationary meanders form, and around the Shatsky Rise agrees with the findings by Mizuno and White (1983), who showed these three regions have maximum rms temperature fluctuations. To the south of the Kuroshio Extension, Figs. 7a–c reveal that there is steady increase in time in the EKE level, a trend we also noticed in Fig. 6d. Notice that this increase occurs over the whole zonal extent of the model basin.

To clarify the causes of these EKE changes in the different regions of the model basin, it is useful to investigate the energetics of the flow field. Equations governing the growth or decay of the EKE and its counterpart in the potential energy, the EPE, have been derived by many investigators. Following Brooks and Niiler (1977), we can write these equations as

$$\frac{\partial}{\partial t}\left[\frac{1}{2}(\overline{u'^2}+\overline{v'^2})\right]+\bar{u}\frac{\partial}{\partial x}\left[\frac{1}{2}(\overline{u'^2}+\overline{v'^2})\right]+\bar{v}\frac{\partial}{\partial y}\left[\frac{1}{2}(\overline{u'^2}+\overline{v'^2})\right]=-\nabla\cdot\frac{\overline{\mathbf{u}'p'}}{\rho_0}-g\frac{\overline{w'\rho'}}{\rho_0}-\overline{u'u'}\frac{\partial\bar{u}}{\partial x}-\overline{u'v'}\frac{\partial\bar{u}}{\partial y}-\overline{v'u'}\frac{\partial\bar{v}}{\partial x}-\overline{v'v'}\frac{\partial\bar{v}}{\partial y}-\overline{w'u'}\frac{\partial\bar{u}}{\partial z}-\overline{w'v'}\frac{\partial\bar{v}}{\partial z}, \quad (4)$$

$$\frac{\partial}{\partial t}\left(\frac{1}{2}\overline{\rho'^2}\right)+\bar{u}\frac{\partial}{\partial x}\left(\frac{1}{2}\overline{\rho'^2}\right)+\bar{v}\frac{\partial}{\partial y}\left(\frac{1}{2}\overline{\rho'^2}\right)=-\overline{u'\rho'}\frac{\partial\bar{\rho}}{\partial x}-\overline{v'\rho'}\frac{\partial\bar{\rho}}{\partial y}-\overline{w'\rho'}\frac{\partial\bar{\rho}}{\partial z}, \quad (5)$$

where overbars denote temporal means and primes the residuals from the mean. On the rhs of Eq. (4), the first term represents the redistribution of energy by the pressure work, the second term, conversions between the EKE and the EPE, and the following four terms, conversions between the EKE and the mean kinetic energy (MKE) due to the horizontal eddy momentum fluxes. The last two terms in Eq. (4) represent the vertical momentum transfer due to small-scale shear instabilities. Likewise, the first two terms on the rhs of Eq. (5) indicate conversions between the EPE and the mean potential energy, and the third term is, again, the conversion term between the EKE and the EPE.

As indicated by Hall (1991) in her study of the Kuroshio Extension from long-term mooring data at 152°E and 35°N, the vertical momentum transfer terms are typically an order-of-magnitude smaller than the leading terms in Eq. (4) and can, thus, be neglected from the following analysis. Since the TOPEX data only provide information on surface velocities, we will focus below on the roles played by the horizontal eddy processes, namely, the barotropic conversion terms

$$\overline{u'u'}\frac{\partial\bar{u}}{\partial x}+\overline{u'v'}\frac{\partial\bar{u}}{\partial y}+\overline{v'u'}\frac{\partial\bar{v}}{\partial x}+\overline{v'v'}\frac{\partial\bar{v}}{\partial y} \quad (6)$$

in changing the EKE level. When the sum of Eq. (6) is negative, the horizontal eddy processes tend to increase the EKE level; in this case, the energy transfer from the MKE to the EKE is associated with barotropic instabilities of the mean flow. On the other hand, positive values of Eq. (6) imply the energy transfer to the mean flow field at the expense of the EKE.

Because the Kuroshio Extension changes its direction and widens as it passes through the model basin, the magnitude and sign of the individual terms in Eq. (6) depend on how one is to define the x-y coordinates (see Hall 1991). Instead of focusing on $\overline{u'v'}\partial\bar{u}/\partial y$ alone, which would be the dominant term if the x coordinate is rotated such that it aligns locally in the direction of the mean flow, we will estimate all terms in Eq. (6) in the conventional east-north coordinates. Notice that the sum of the barotropic conversion terms is independent of the coordinate system.

To compute the velocity autocovariances ($\overline{u'u'}$, $\overline{v'v'}$) and the velocity cross-covariance $\overline{u'v'}$, we use the residual SSH data after objective mapping (i.e., the SSH data shown in Fig. 5 but without the mean field added). Velocity residuals are calculated from these residual SSH data by assuming geostrophy. Given the track distribution of Fig. 1, it is clear that the estimation for the velocity cross-covariance is more accurate near the crossover points, where both u' and v' are more accurately measured. Due to this restriction, as well as the fact that the changes in the EKE seem to occur coherently in the downstream direction (see Fig. 7), we will focus our discussions below on quantities that

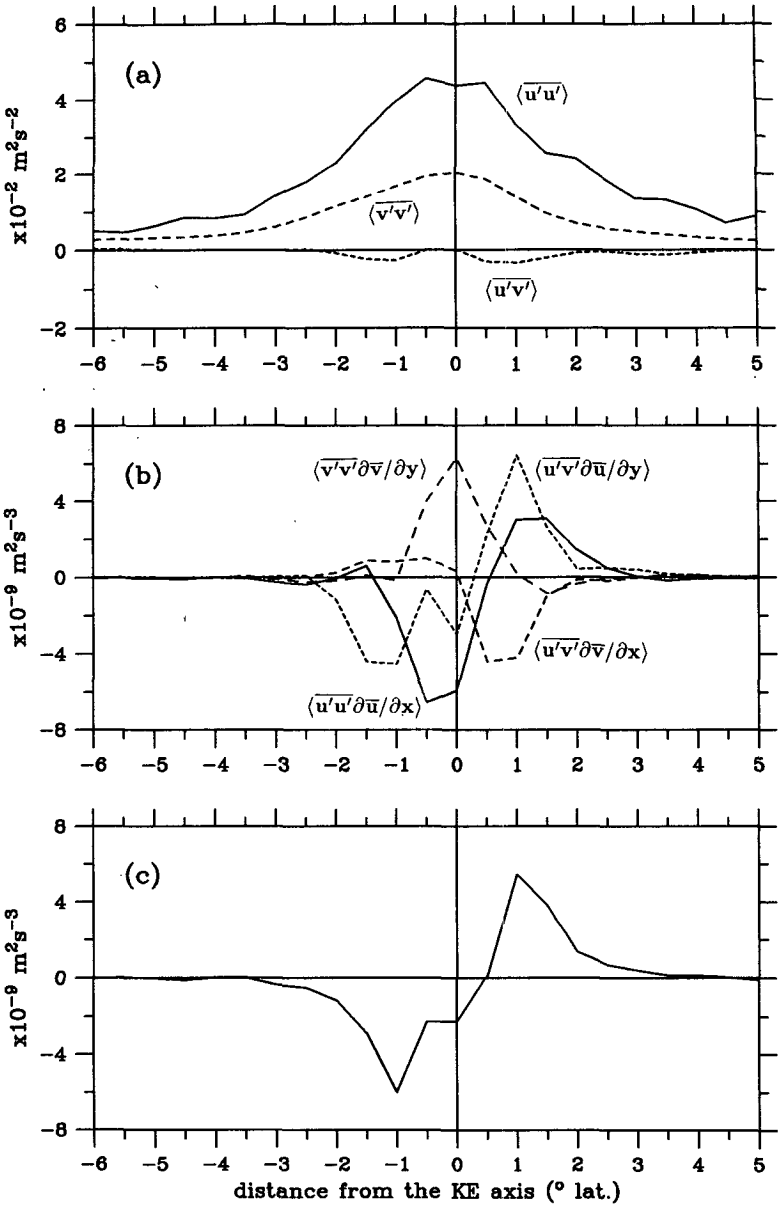

FIG. 8. (a) Cross-stream velocity covariances $\langle \overline{u'u'} \rangle$, $\langle \overline{v'v'} \rangle$, and $\langle \overline{u'v'} \rangle$ plotted as a function of distance away from the mean Kuroshio Extension axis (i.e., the 2.38-m contour in Fig. 4). (b) Cross-stream profiles of the four barotropic conversion terms in Eq. (7). (c) Cross-stream profile of the sum of the barotropic conversion terms. All values shown in (a)–(c) have been averaged along the mean path of the Kuroshio Extension from 136°E to 180°.

are averaged along the mean path of the Kuroshio Extension (denoted below by $\langle \quad \rangle$).

Figure 8a shows the velocity covariances $\langle \overline{u'u'} \rangle$, $\langle \overline{v'v'} \rangle$, and $\langle \overline{u'v'} \rangle$ as a function of northward distance away from the mean Kuroshio Extension axis. Notice that the velocity cross-covariance $\langle \overline{u'v'} \rangle$ is negative on both sides of the Kuroshio Extension during the two-year period of the TOPEX mission. Using the first-year Geosat ERM data, Tai and White (1990) have looked into the residual velocity cross-covariance; they showed that $\langle \overline{u'v'} \rangle < 0$ north of the Kuroshio Extension and $\langle \overline{u'v'} \rangle > 0$ to the south. This same trend is found in the study by Nishida and White (1982), who investigated the horizontal eddy fluxes using historical XBT data. For the Kuroshio south of Japan, on the other hand, Szabo and Weatherly (1979) found the opposite cross-stream structure for $\langle \overline{u'v'} \rangle$ (i.e., $\langle \overline{u'v'} \rangle < 0$ to

the south). It is worth emphasizing that the cross-stream structure of $\overline{u'v'}$ does not need to be time invariant: long-term mooring observations by Schmitz et al. (1987) along 152°E showed that the sign of $\overline{u'v'}$ across the Kuroshio Extension could change from year to year.

Figure 8b shows the cross-stream profiles of the four barotropic conversion terms. Similar to the result found by Nishida and White (1982), there is a tendency for $\langle \overline{u'u'}\partial\bar{u}/\partial x\rangle$ and $\langle \overline{v'v'}\partial\bar{v}/\partial y\rangle$ to cancel each other at each cross-stream location, a tendency due to the near-isotropic nature of the residual velocity field. For the other two terms, $\langle \overline{u'v'}\partial\bar{u}/\partial y\rangle$ is dominant as expected, though contribution from $\langle \overline{u'v'}\partial\bar{v}/\partial x\rangle$ is significant, especially north of the Kuroshio Extension. This latter term is important because the mean flow of the Kuroshio Extension diverges to the east and contains a number of quasi-stationary meanders (Nishida and White 1982).

The sum of the barotropic conversion terms, shown in Fig. 8c, indicates that during the first two-year TOPEX mission, the horizontal eddy processes work to increase the EKE level south of the Kuroshio Extension and to decrease it north of the Kuroshio Extension. By separating the residual SSH data into different regions, we have shown above that the EKE level increases more or less steadily in the region south of the Kuroshio Extension (Fig. 6d). This trend to increase is consistent with the result that the barotropic conversion there is negative. To see whether the observed conversion rate is on the same order as the increasing rate of the EKE, we averaged the conversion rates in Fig. 8c in the region 1.5° south of the Kuroshio Extension (recall the width of the Kuroshio Extension was assumed to be 3° in latitude). The result is -0.29×10^{-9} m^2 s^{-3}. With the sign reversed, this value is close to the increasing rate of the EKE, 0.256×10^{-9} m^2 s^{-3}, from the least-squares fit. This suggests that the barotropic instability of the mean circulation is a likely mechanism for the increase in the EKE level in the southern recirculation gyre region during the first two-year TOPEX mission.

In the Kuroshio Extension and the region to the north, the spatially averaged barotropic conversion rates are -0.71×10^{-9} m^2 s^{-3} and 0.48×10^{-9} m^2 s^{-3}, respectively. Clearly, these values cannot explain the EKE changes found in Figs. 6c and 6b; in the Kuroshio Extension there is an apparent decrease in the EKE level over the two-year TOPEX mission, whereas no linear trend as we found above is apparent in the northern region. For these regions, this study suggests that energy sources other than the barotropic conversion are responsible for the observed EKE changes. Because the model domain of this study is not closed, one candidate for the EKE changes can be the mean flow advection through open boundaries [i.e., by the advective terms on the lhs of Eq. (4)]. Estimating these terms in the Kuroshio Extension and its northern regions from the TOPEX data reveals that they account for 0.08×10^{-9} m^2 s^{-3} and -0.01×10^{-9} m^2 s^{-3} of the EKE changes, both of which are about an order-of-magnitude smaller than the barotropic conversion terms.

A more likely candidate for the observed EKE changes in the Kuroshio Extension and its northern regions is the energy transfer due to baroclinic instabilities. Although lack of simultaneous surface density observations prevents us from estimating the baroclinic conversion terms in Eqs. (4) and (5), many previous studies have found the baroclinic instability to be the major energy source for the variability of an eastward-flowing boundary jet (e.g., Holland and Haidvogel 1980; Ikeda 1981; and Wood 1988). Because the meridional density gradient is largest along the northern flank of the Kuroshio Extension (e.g., Niiler et al. 1985), it is conceivable that the baroclinic energy transfer is most effective in the Kuroshio Extension and its northern regions.

5. Low-frequency variations in the Kuroshio Extension and its recirculation gyre

From the kinematic jet model described in section 3, we now have time series for the position of the Kuroshio Extension axis $a_2(t)$ and the SSH difference across the Kuroshio Extension,

$$\delta h_{\mathrm{KE}} = \frac{f}{g}\sqrt{2\pi}a_1(t)a_3(t), \tag{7}$$

along individual ground tracks. This latter quantity, as found in Kelly and Watts (1994) for the Gulf Stream, has a high correlation with the baroclinic transport in the upper thermocline of an eastward-flowing boundary current extension. Rather than focusing on the evolution and propagation of individual meanders of the Kuroshio Extension, we will confine our discussion in this section to the zonally averaged, low-frequency changes in the path and surface transport of the Kuroshio Extension.

Figure 9a shows the time series for the position of the Kuroshio Extension's axis zonally averaged from 140°E to 180°. The time series for the zonally averaged δh_{KE} is shown in Fig. 9b. Over the first two-year period of the TOPEX mission, there is a clear trend for the (zonal) mean path of the Kuroshio Extension to migrate southward (by 1° over the two years). Accompanying this southward migration is the decrease in the Kuroshio Extension's surface transport. The decrease in δh_{KE} over the two-year period is 0.2 m, which is a 25% reduction in the surface transport. In addition to this long-term trend, the two time series also have apparent seasonal cycles: the Kuroshio Extension has a relatively large surface transport in fall and winter when it is located relatively north as compared to the spring and summer seasons when it is located more

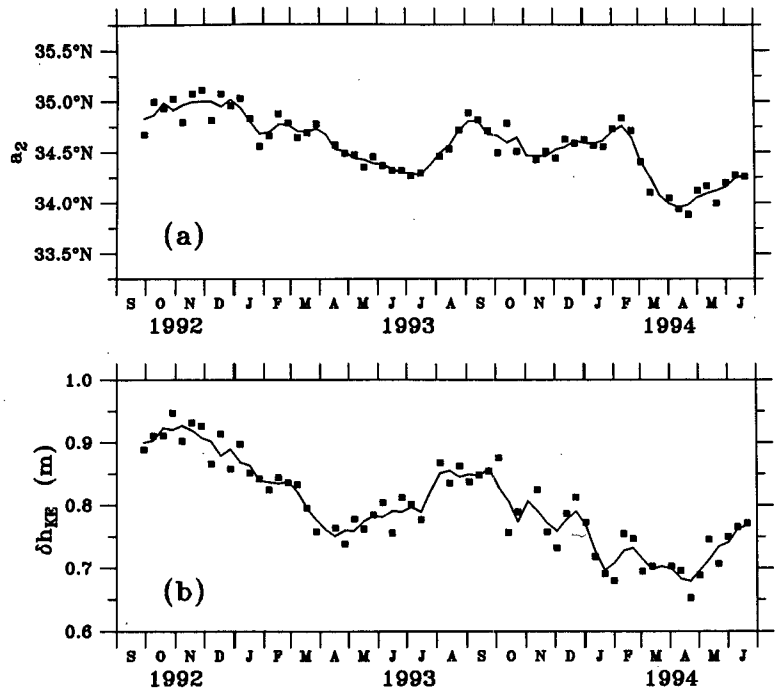

FIG. 9. Time series of (a) the zonally averaged axis position of the Kuroshio Extension and (b) the zonally averaged SSH difference across the Kuroshio Extension. Here, zonal averages are taken from 140°E to 180° after the point of separation of the Kuroshio from the coast of Japan. Solid marks denote values from individual TOPEX cycles and solid lines denote averages over the consecutive three cycles.

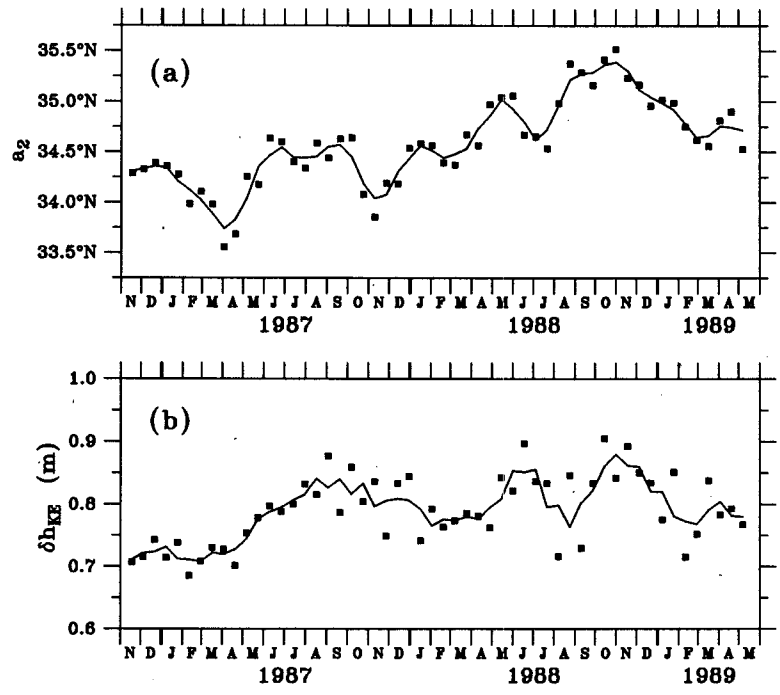

FIG. 10. Same as in Fig. 9 except for the data from the Geosat Exact Repeat Mission (see Qiu et al. 1991). The Geosat altimeter has a repeat cycle of 17 days.

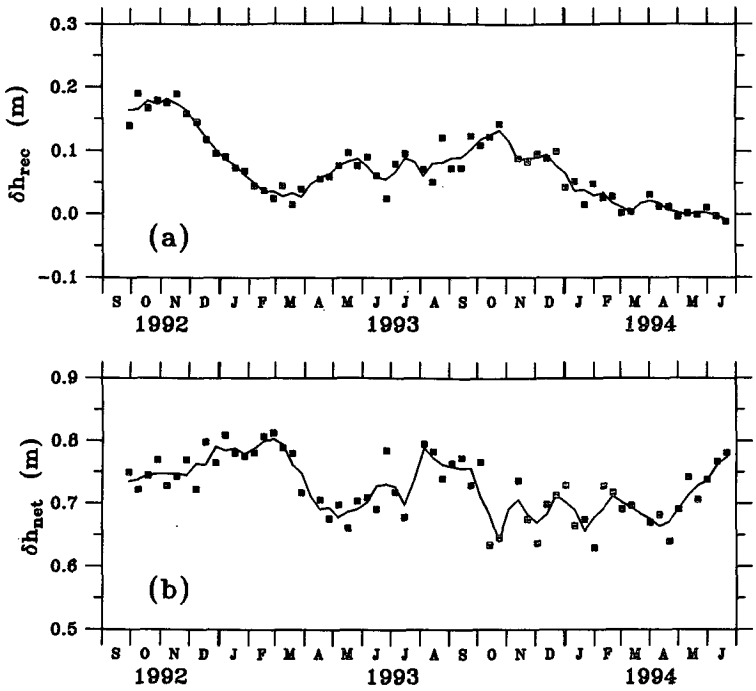

FIG. 11. (a) Time series of the zonally averaged SSH difference across the southern recirculating flow of the Kuroshio Extension. Here, the SSH difference is defined by Eq. (9). (b) Time series of the zonally averaged SSH difference across the entire Kuroshio Extension system, that is, the eastward-flowing Kuroshio Extension and its westward recirculating flow; $\langle \delta h_{net} \rangle = \langle \delta h_{KE} \rangle - \langle \delta h_{rec} \rangle$.

southward. A linear regression shows that the linear correlation coefficient between the two time series is high at 0.74. For the estimated 7 degrees of freedom in the time series, this value is significant at a 90% confidence level.

For comparison, we show in Figs. 10a and 10b the time series of $\langle a_2 \rangle$ and $\langle \delta h_{KE} \rangle$ using the data from the Geosat ERM. Although the trend in the time series during the first 2-year period of the Geosat ERM (November 1986–October 1988) has an opposite sign to that shown in Figs. 9a and 9b, the positive correlation between a more northerly Kuroshio Extension and a larger surface transport remains unchanged. The seasonal signals in the Geosat ERM period are essentially the same as those found in Fig. 9. The fact that the SSH jump across the Kuroshio Extension is higher in the fall than in other seasons during the period of Geosat ERM has been previously noted by Tai (1990), Qiu et al. (1991), Zlotnicki (1991), and Mitchell et al. (1994). Notice that the positive correlation between the boundary current extension's path and surface transport has also been detected in the Gulf Stream for the Geosat ERM period (Kelly 1991).

To clarify the causes for these observed large-scale, low-frequency changes, it is helpful here to look into the changes in the recirculating flows south of the Kuroshio Extension. As we noted in the introduction, the downstream transport increase of the Kuroshio and the Kuroshio Extension is associated with the presence of the westward recirculating flows. It is, thus, not surprising that the low-frequency fluctuations of the Kuroshio Extension could be connected to the fluctuations of its southern recirculating flows. To look into this connection, we define the strength of the westward recirculating flows by

$$\delta h_{rec} = ssh^{north} - ssh^{south}, \tag{8}$$

where ssh^{south} is the absolute SSH value (residual + the mean) averaged over a 2° segment from 25° to 27°N along a ground track, and ssh^{north} is the value averaged over a 2° segment immediately south of the Kuroshio Extension, namely, from $a_2(t) - 3.5°$ to $a_2(t) - 1.5°$. Here, averaging over a 2° segment is taken to remove small-scale errors in the residual SSH data.

Figure 11a shows the time series of the $\langle \delta h_{rec} \rangle$ values zonally averaged from 140°E to 180°. By comparing this time series with that of Fig. 9b, it is obvious that the fluctuations in the surface transport of the Kuroshio Extension are highly correlated with those of the recirculating flows ($r = 0.74$). For example, the fall/winter increase in $\langle \delta h_{KE} \rangle$ is accompanied by the intensification in the westward recirculating flows (i.e., larger $\langle \delta h_{rec} \rangle$ values) in these same seasons. Similarly, the interannual trend has the same sign and amplitude in Fig. 11a as in Fig. 9b. Notice that the high correlation between $\langle \delta h_{KE} \rangle$ and $\langle \delta h_{rec} \rangle$ suggests that the SSH dif-

ference across the entire Kuroshio Extension system, namely, the eastward-flowing Kuroshio Extension plus its southern recirculating flows, has no coherent, low-frequency changes. This, in fact, is the case as shown in Fig. 11b. Since the SSH difference across the entire Kuroshio Extension system $\langle \delta h_{\mathrm{net}} \rangle$ is a quantity that is controlled by the inflow of the North Pacific subtropical gyre, the above result implies that the seasonal and interannual fluctuations of the Kuroshio Extension observed during the TOPEX mission are more of a regional origin than a consequence of basin-scale external forcings.

Following Worthington (1976), if we regard the southern recirculation gyre as an anticyclonic circulation encompassing the westward recirculating flow and a part of the eastward-flowing Kuroshio Extension, the result of Figs. 9b and 11a simply indicates that this southern recirculation gyre weakened steadily over the first two-year period of the TOPEX mission. This finding is consistent with the result discussed in the previous section. By computing the barotropic conversion terms in the energy equation, we found that the energy transfer in regions south of the Kuroshio Extension was from the mean flow field to the eddy field. Such an energy depletion in the mean flow field is likely to cause the spindown of the Kuroshio Extension's southern recirculation gyre, the result found in Figs. 9b and 11a.

6. Conclusions

Using the altimeter data from the first two-year TOPEX mission, we investigated the SSH fluctuations in the regions of the Kuroshio Extension and its southern recirculation gyre. The focus of the study has been on the energy transfers that control the EKE fluctuations and on the large-scale, low-frequency changes in the path and surface transport of the Kuroshio Extension and the southern recirculating flows. Answering both of these questions requires information about the mean SSH field. To study energy transfers, for example, the mean surface velocity field is necessary for evaluating the barotropic conversion terms. Similarly, the mean SSH field is needed to separate the residual SSH fluctuations associated with the Kuroshio Extension from those associated with the recirculating flows.

To obtain the mean SSH field that is pertinent to the first two-year period of the TOPEX mission, we extended the kinematic jet model of Kelly and Gille (1990) to include the effects from the westward recirculating flows. This is done by allowing for the existence of the mean SSH slopes away from the Kuroshio Extension and by constraining the net height difference across the entire Kuroshio Extension system (25°–40°N) using climatological hydrographic data. The mean SSH field thus estimated exhibits a sharper cross-stream structure of the Kuroshio Extension and a more intensified southern recirculation gyre than in the Levitus (1982) climatology. The general pattern of the mean SSH field agrees well with the patterns estimated previously by Mizuno and White (1983) and by Teague et al. (1990).

During the two-year period of the TOPEX mission, the EKE levels changed differently in different regions of the Kuroshio Extension system. Inside the band of the eastward-flowing Kuroshio Extension, the EKE level increased 10% in the period from April to November of 1993, as compared to the previous 6 months from October 1992 to March 1993. After December of 1993, the EKE level dropped significantly from a mean value of 0.16 $m^2 s^{-2}$ to 0.12 $m^2 s^{-2}$. The EKE level in the region south of the Kuroshio Extension, on the other hand, increased more or less steadily over the past two-year period; the increase rate is about 0.008 $m^2 s^{-2}$ (or 0.09 $m s^{-1}$ in rms velocity) per year.

To clarify the possible causes for these observed EKE changes, we estimated the barotropic conversion rate using the residual SSH data and the synthetic mean height field reconstructed from the kinematic jet model. For the region south of the Kuroshio Extension, we found that the horizontal eddy processes tended to transfer kinetic energies from the mean flow field to the eddy field. The energy conversion rate due to the horizontal eddy processes is about 0.009 $m^2 s^{-2}$, which is on the same order as the increase rate of the EKE estimated from the residual SSH data. This result suggests that the barotropic instability is a possible cause for the EKE increase observed in the southern recirculation gyre. The barotropic conversion, however, can not account for the EKE changes observed within the Kuroshio Extension and in the region north of the Kuroshio Extension. In these regions, other energy sources, such as the baroclinic instabilities, are expected to be important.

To extract the low-frequency, coherent signals and reduce the influence from mesoscale eddies, we examined the path and surface transport fluctuations of the Kuroshio Extension by zonal averaging. On both seasonal and interannual timescales, there exists a positive correlation between the fluctuations of the Kuroshio Extension's path and its surface transport. In other words, a more northerly current path tends to correspond to a larger surface transport. This same correlation has also been observed in the Gulf Stream (Kelly 1991) and the Kuroshio Extension (Qiu et al. 1991) from the Geosat ERM data.

On the interannual timescale, the surface transport of the Kuroshio Extension decreased steadily over the two-year period of the TOPEX mission. In accordance with this decrease in the eastward transport is the weakening in the westward recirculating flows. The fact that the decreases in these two flows have similar magnitudes suggests that there is a steady decline in the strength of the southern recirculation gyre of the Kuroshio Extension during the 2-year period of the TOPEX mission. From the study of energetics, we note that this decline in the southern recirculation gyre may

be a result due to the kinetic energy transfer from the mean flow field to the eddy field during this time period.

The strong coupling between the Kuroshio Extension and its southern recirculation gyre implies that the observed low-frequency fluctuations in the Kuroshio Extension system are possibly caused by the regional surface forcings as opposed to basin-wide external forcings. This postulation is supported by a recent study by Kelly et al. (1994), in which they conducted canonical correlation analyses and found that the second wind stress EOF mode in the Kuroshio Extension region was significantly correlated with the Kuroshio Extension's surface transport mode during the 2.5 years of Geosat ERM. Regions of large wind stress anomalies generally corresponded to regions of large surface transport anomalies.

A related question not yet answered is why the path fluctuations of the Kuroshio Extension synchronize with those in the surface transport. We speculate that as the southern recirculation gyre is spun up by the stronger-than-usual regional wind, the Kuroshio Extension gains its strength and tends to expand northward at the same time. A recent work by Jacobs et al. (1994) has proposed a different mechanism behind the interannual fluctuations of the Kuroshio Extension path. They suggested that the northward path shift over the period of April 1992–March 1993 (ERS-1 mission), as compared to November 1986–October 1989 (Geosat ERM), was due to the westward passage of warm Rossby waves that had their origins in the 1982/83 ENSO event. Clearly, the two-year TOPEX data at this point are still too short to ascertain the causes of the observed low-frequency changes. To answer the questions raised above, future studies based on longer altimetric measurements and using numerical models that resolve both the detailed dynamics of the Kuroshio Extension and the basin-scale ocean circulation are required.

Acknowledgments. Discussions with Kathryn Kelly, Mark Saunders, and Gary Mitchum have clarified many parts of the present work. Melinda Hall and an anonymous reviewer carefully read an early version of the manuscript and made many helpful comments. The TOPEX data were obtained from the Physical Oceanography DAAC at Jet Propulsion Laboratory, California Institute of Technology. I am grateful for the help in the management and processing of the original TOPEX data by the University of Hawaii Sea Level Center. This work was supported by the Office of Naval Research through Grant N00014-92-J-1656.

REFERENCES

Brooks, I. H., and P. P. Niiler, 1977: Energetics of the Florida Current. *J. Mar. Res.*, **35**, 163–191.

Callahan, P. S., 1993: *TOPEP/POSEIDON GDR Users Handbook.* Jet Propulsion Laboratory, Special publication D-8944, 84 pp.

Hall, M. M., 1989: Velocity and transport structure of the Kuroshio Extension at 35°N, 152°E. *J. Geophys. Res.*, **94**, 14 445–14 459.

——, 1991: Energetics of the Kuroshio Extension at 35°N, 152°E. *J. Phys. Oceanogr.*, **21**, 958–975.

Holland, W. R., and D. B. Haidvogel, 1980: A parameter study of the mixed instability of idealized ocean currents. *Dyn. Atmos. Oceans*, **4**, 185–215.

Ikeda, M., 1981: Meanders and detached eddies of a strong eastward-flowing jet using a two-layer quasi-geostrophic model. *J. Phys. Oceanogr.*, **11**, 526–540.

Jacobs, G. A., H. E. Hurlburt, J. C. Kindle, E. J. Metzger, J. L. Mitchell, W. J. Teague, and A. J. Wallcraft, 1994: Decade-scale trans-Pacific propagation and warming effects of an El Nino warming anomaly. *Nature*, **370**, 360–363.

Joyce, T. M., and W. J. Schmitz Jr., 1988: Zonal velocity structure and transport in the Kuroshio Extension. *J. Phys. Oceanogr.*, **18**, 1484–1494.

Kawabe, M., 1985: Sea level variations at the Izu Islands and typical stable paths of the Kuroshio. *J. Oceanogr. Soc. Jpn.*, **41**, 307–326.

Kawai, H., 1972: Hydrography of the Kuroshio Extension. *Kuroshio—Its Physical Aspects*, H. Stommel and K. Yoshida, Eds., University of Tokyo Press, 235–354.

Kelly, K. A., 1991: The meandering Gulf Stream as seen by the Geosat altimeter: Surface transport, position, and velocity variance from 73° to 46°W. *J. Geophys. Res.*, **96**, 16 721–16 738.

——, and S. T. Gille, 1990: Gulf Stream surface transport and statistics at 69°W from the Geosat altimeter. *J. Geophys. Res.*, **95**, 3149–3161.

——, and D. R. Watts, 1994: Monitoring Gulf Stream transport by radar altimeter and inverted echo sounders. *J. Phys. Oceanogr.*, **24**, 1080–1084.

——, M. J. Caruso, S. Singh, and B. Qiu, 1994: Observations of atmosphere/ocean coupling in western boundary currents. *J. Geophys. Res.*, submitted.

Levitus, S., 1982: *Climatological Atlas of the World Ocean.* NOAA Prof. Paper No. 13, U.S. Govt. Printing Office, Washington, DC, 173 pp.

Masuzawa, J., 1972: Water characteristics of the North Pacific central region. *Kuroshio—Its Physical Aspects*, H. Stommel and K. Yoshida, Eds., University of Tokyo Press, 95–128.

Mitchell, J. L., W. J. Teague, G. A. Jacobs, H. E. Hurlburt, and P. J. Hogan, 1994: Comparisons of eddy-resolving model simulations and Geosat-ERM altimetry in the Kuroshio Extension. *J. Geophys. Res.*, **99**, in press.

Mitchum, G. T., 1994: Comparison of TOPEX sea surface heights and tide gauge sea levels. *J. Geophys. Res.*, **99**, 24 541–24 553.

Mizuno, K., and W. B. White, 1983: Annual and interannual variability in the Kuroshio Current system. *J. Phys. Oceanogr.*, **13**, 1847–1867.

Niiler, P. P., W. J. Schmitz Jr., and D. K. Lee, 1985: Geostrophic volume transport in high eddy-energy areas of the Kuroshio Extension and the Gulf Stream. *J. Phys. Oceanogr.*, **15**, 825–843.

Nishida, H., and W. B. White, 1982: Horizontal eddy fluxes of momentum and kinetic energy in the near-surface of the Kuroshio Extension. *J. Phys. Oceanogr.*, **12**, 160–170.

Qiu, B., 1992: Recirculation and seasonal change of the Kuroshio from altimetric data. *J. Geophys. Res.*, **97**, 17 801–17 811.

——, and K. A. Kelly, 1993: Upper ocean heat balance in the Kuroshio Extension region. *J. Phys. Oceanogr.*, **23**, 2027–2041.

——, ——, and T. M. Joyce, 1991: Mean flow and variability in the Kuroshio Extension from Geosat altimetry data. *J. Geophys. Res.*, **96**, 18 491–18 507.

Schmitz, W. J., Jr., P. P. Niiler, and C. J. Koblinsky, 1987: Two-year moored instrument results along 152°E. *J. Geophys. Res.*, **92,** 10 826–10 834.

Suga, T., K. Hanawa, and Y. Toba, 1989: Subtropical mode water in the 137°E section. *J. Phys. Oceanogr.*, **19,** 1605–1618.

Szabo, D., and G. C. Weatherly, 1979: Energetics of the Kuroshio south of Japan. *J. Mar. Res.*, **37,** 531–556.

Taft, B., 1972: Characteristics of the flow of the Kuroshio. *Kuroshio—Its Physical Aspects,* H. Stommel and K. Yoshida, Eds., University of Tokyo Press, 165–216.

Tai, C.-T., 1990: Estimating the surface transport of meandering oceanic jet streams from satellite altimetry: Surface transport estimates for the Gulf Stream and Kuroshio Extension. *J. Phys. Oceanogr.*, **20,** 860–879.

——, and W. B. White, 1990: Eddy variability in the Kuroshio Extension as revealed by Geosat altimetry: Energy propagation away from the jet, Reynolds stress, and seasonal cycle. *J. Phys. Oceanogr.*, **20,** 1761–1777.

Teague, W. J., M. J. Carron, and P. J. Hogan, 1990: A comparison between the Generalized Digital Environmental Model and Levitus climatologies. *J. Geophys. Res.*, **95,** 7167–7183.

Wood, R. A., 1988: Unstable waves on oceanic fronts: Large amplitude behavior and mean flow generation. *J. Phys. Oceanogr.*, **18,** 775–787.

Worthington, L. V., 1976: On the North Atlantic circulation. *Johns Hopkins Oceanogr. Stud.*, **6,** 110 pp.

Zlotnicki, V., 1991: Sea level differences across the Gulf Stream and Kuroshio Extension. *J. Phys. Oceanogr.*, **21,** 599–609.